Finite-Size Effects on the Closest Packing of Hard Spheres

S. Neser, C. Bechinger, and P. Leiderer
Fakultät für Physik, Universität Konstanz, D-78434 Konstanz, Germany

T. Palberg
Institut für Physik, Universität Mainz, D-55099 Mainz, Germany
(Received 13 June 1997; revised manuscript received 11 August 1997)

We study closely packed crystalline structures formed by slow lateral compression of a colloidal suspension of hard spheres in a thin wedge. In addition to the known sequence of structural transitions, a buckling mechanism was recently proposed to maximize the packing fraction Φ between one and two layers. We here confirm this prediction experimentally and present the first evidence that for more than two layers, buckling, in this case of prism shaped arrays of particles, also takes place. This efficient mechanism may enhance Φ by up to 4% and dominates in major regions of the phase diagram. [S0031-9007(97)04068-4]

PACS numbers: 82.70.Dd, 61.72.Nn, 81.30.–t

The close packing of hard spheres has a long-standing history in the explanation of natural shapes. Kepler [1], e.g., was the first who suggested a hexagonal close packed arrangement of tiny ice spheres to account for the sixfold symmetry of snowflakes. The importance of closest sphere packings for both fundamental research, e.g., crystallography and solid state physics, as well as for more applied topics like communication science [2] or modern powder and sinter technology, reflects itself in an immense amount of literature [3].

While it was proven already by Gauss [4] that the face centered cubic (fcc) crystal structure (besides its derivatives, hexagonal close packing and random close stackings) is the closest *crystalline* packing ($\Phi_{\mathrm{fcc}} = \frac{\pi}{3\sqrt{2}} \approx 0.74$) in three dimensions (3D), only recently there is a—still controversially discussed—proof for fcc to be the closest sphere packing at all [5]. The difficulty is that partial packings with higher Φ exist [6] and one has to prove that this local arrangement cannot be continued in a way that its global Φ exceeds Φ_{fcc}.

The situation gets even more difficult when finite-size effects [7], arising from a confined geometry, are considered: Even in the less complicated two-dimensional case, most finite-size packing problems are not solvable analytically and numerical solutions request huge amounts of computer time [8].

A completely different, alternative approach to attack such problems is to study the crystallization behavior of micron sized colloidal spheres suspended in water. Because of their Brownian motion, the spheres are efficiently sampling their configuration space and quickly reach thermodynamic equilibrium. In systems with high internal pressure this can be expected to maximize Φ, and therefore colloidals can be utilized as *analog computers* to find dense sphere packings. Furthermore, both the typical time (seconds) and length scales (micrometers) are accessible by video microscopy and allow the accurate determination of structural and dynamic quantities [9].

This method has been used to investigate structure formation in confined geometries by a number of authors [10,11], who investigated the transition between 2D and 3D with colloidal particles confined in a wedge. Starting with one hexagonal monolayer at small wall separations, with increasing wedge height a sequence of morphological transitions was found:

$$n\triangle \rightarrow (n+1)\square \rightarrow (n+1)\triangle, \qquad (1)$$

where n is the number of layers and $\square$ and $\triangle$ correspond to layers of quadratic and hexagonal symmetry, respectively. The sequence can be understood considering the fact that the height of a fcc stack with quadratic (100) layers is smaller than that of the corresponding hexagonal (111) stack, and that Φ rapidly decreases when a particular stack does not exactly match the cell height. Thus, with increasing cell height the (100) stack fits first between the walls and is later replaced by the (111) phase in order to maintain a high Φ. However, for a quantitative description of the phase boundaries, also distortions of the fcc lattice have to be considered.

Pansu *et al.* [12] suggested an additional mechanism, known as buckling, which optimizes Φ during the transition between $1\triangle$ and $2\square$ even further: In the presence of lateral forces, single lattice rows can be vertically displaced out of a hexagonal monolayer and a folded structure forms which leads smoothly into the $2\square$ structure [Fig. 1(a)]. Additionally, the model proposed a smooth transition between $2\square$ and $2\triangle$ via a phase with rhombic symmetry. Evidence for both features was found experimentally [13–15] as well as in Monte Carlo simulations [16] and in a stability analysis [17] of the 2D hexagonal lattice. However, although the buckling principle turns out to be an important mechanism to maximize Φ during the transition from $n = 1$ to $n = 2$, only little is known about its extension to the transitions with higher n.

In our experiments we investigate the crystallization of a colloidal suspension of nearly hard spheres in a

 0031-9007/97/79(12)/2348(4)$10.00

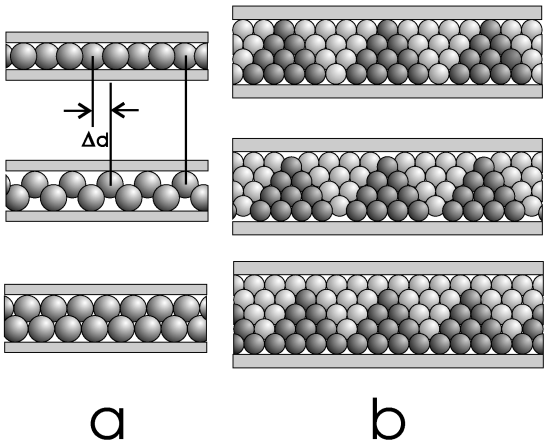

FIG. 1. (a) Buckling transition between 1△ (top) and 2□ (bottom). The middle picture shows the situation when the wall separation is larger than the sphere diameter σ but not sufficient to allow for the 2□ phase. The arrangement of the spheres in the suggested way (buckling) decreases the projection of the sphere distance on the *x-y* plane by Δd and therefore increases the packing fraction Φ. (b) Buckling transition involving a larger number of layers. As in (a), the cell height increases from the upper to the lower picture. The top, middle, and bottom pictures show cross sections (111 planes) of the 4□, 4$\mathcal{P}$, and 5□ structures, respectively, and the different shadings are guides to the eye for a better distinction between the prisms. Similar as in the buckling transition in (a) it can be seen from the middle picture that the buckling of the prisms allows one to pack a considerably larger number of spheres between the walls.

wedge geometry. In contrast to the former work, in our experiments a small flow of the solvent was utilized to establish a gradient in the particle density and to compress the particles into a dense colloidal solid. We find a sequence of structural transitions similar to that described above but with a considerably larger number of phases. We present evidence for these phases to be an implementation of the buckling principle for structures with more than one monolayer.

To obtain a well-defined wedge we used two optically flat quartz glass plates and placed 4.5 μm polystyrene (PS) spheres as spacers along a rim of one of them. Then the plates were assembled and fixed with epoxy glue, leaving several small holes. Afterwards we applied a droplet of suspension to one of the holes and waited until the wedge had filled due to capillarity. Finally the complete cell was sealed with epoxy. We used surfactant stabilized PS spheres with a diameter σ of 842 nm (Bangs Labs Lot: 20PS196). A videomicroscopic measurement of the radial distribution function $g(r)$ of a single fluid monolayer showed an effective hard spherelike behavior with the first peak located at 1.2σ. To determine the absolute height profile the wedges were characterized by means of two-wavelength laser interferometry. The wedge angle typically was on the order of 10^{-4} rad corresponding to a height variation of only 20 nm over a distance of 100σ. Therefore the cell walls can be considered to be locally parallel. Since the epoxy seal as prepared in our experiments has a small permeability for water, the diffusion of liquid through the seal produces an—albeit very small—flow of the suspension toward the edges of the wedge, where Φ increases because the epoxy is impenetrable for the spheres. When the volume fraction exceeds the hard sphere freezing concentration the system starts to crystallize and during the evaporation process (taking up to one week) the phase boundary moves slowly through the cell.

The resulting solid consists of small crystallites with typical sizes between 10 and 50 particle diameters. The structures were investigated with an inverse optical microscope and a scanning electron microscope (SEM). For the latter, after complete evaporation of the solvent, we carefully removed the top plate of some wedges and sputtered a thin layer of gold on top of them. It turned out that the cohesion forces between the particles are larger than those between the particles and the substrate, so that sufficiently large areas of the sample remained undamaged by this procedure.

The observation of the sample with the optical microscope shows that the microstructure of the crystallites depends on the local wedge height z. Starting with small wall separations we find a monolayer with hexagonal symmetry (1△). When z increases, a smooth transition into the quadratic phase (2□) via the above mentioned buckling mechanism (1$\mathcal{B}$) is observed [cf. Fig. 1(a)]. In the 1$\mathcal{B}$ phase the hexagonal layer is split into two sublayers separated by a fraction of $z_{2\square}$, the height of the 2□ phase. Within each sublayer the particles are arranged in rows. In the range of the buckling transition the distance of the sublayers increases and the separation of adjacent rows within a sublayer gets smaller. The whole scenario is depicted in Fig. 1(a). The exploitation of the additional volume, produced by the increasing wall separation, allows one to decrease the projection of the sphere separation onto the *x-y* plane and therefore to increase Φ. The buckling process is completed when adjacent rows in each sublayer touch each other, corresponding to the 2□ phase.

In agreement with the phase diagram given by Schmidt and Löwen [16] 2□ then is followed by the rhombic $\mathcal{R}$ and the 2△ phase, as identified by microscopy. With z increasing further we find the situation shown in Fig. 2, where the wedge height increases from right to left. There is a sharp boundary between 2△ and a region with quadratic symmetry. Directly at the phase boundary a pronounced stripe pattern is visible which, with increasing distance from the boundary, decays continuously into a purely quadratic structure (3□). Similar stripe patterns are found each time a new monolayer is added. In the following we discuss the structure of the striped regions in detail: Figure 3(a) shows a SEM picture of the transition region between 4△ and 5□. The surfaces of the crystallites correspond to (100) planes, being disrupted

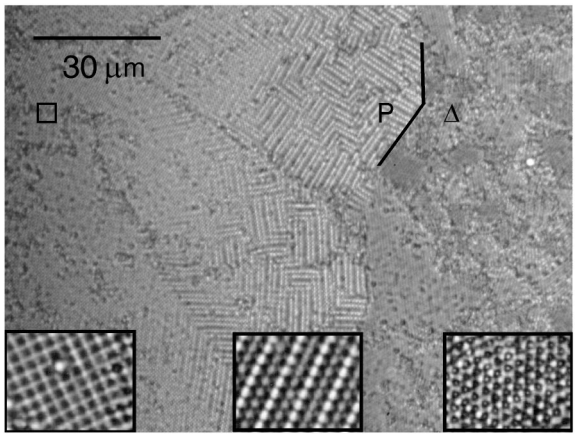

FIG. 2. Optical micrograph of the transition region between 2△ and 3□. The wedge height increases from right to left and the black lines in the upper right corner indicate the sharp boundary between △ and $\mathcal{P}$ which is followed by the smooth decay of 3$\mathcal{P}$ into 3□. The insets show more detailed views of the △, $\mathcal{P}$, and □ regions as observed with the optical microscope.

every four particles along one direction by a row of spheres which lies below the others and which is also displaced by half a particle diameter in the direction of the rows. On the left side, where the spheres have been removed during the disassembly of the wedge, a cross section of the structure is revealed. The enlargement of this region [Fig. 3(b)] shows that the structure is composed of triangular shaped prisms (four spheres on each side) which are interlocked. We found such prisms with side lengths ranging between two and up to eight particle diameters σ, at locations where the wedge heights allow for two to eight monolayers. In the following they will be referred to as *n*-layer *prism phases* $n\mathcal{P}$.

To analyze the properties of the new phases we considered rigid prisms with an equal number of particles at each side: If, as implied by Fig. 3(b), the base of a prism is a (100) plane, then the side planes have to be (111) planes in order to obtain an equal number of particles on each side of the prism. Therefore there are two possibilities to interlock the sides of two adjacent prisms. On one hand one can keep the fcc stacking scheme ($abca\ldots$) leading to a quadratic symmetry. On the other hand, introducing a stacking fault, the prisms can also be interlocked in the hcp scheme ($aba\ldots$). It is the latter that reproduces the structure of Fig. 2. The height of the $n\mathcal{P}$ phase is then calculated to be

$$z_{n\mathcal{P}} = z_{n\square} + \frac{1}{3\sqrt{2}}\,\sigma\,, \tag{2}$$

where σ is the diameter of the spheres and $z_{n\square}$ the height of the $n\square$ structure. An analysis of $\Phi_{n\mathcal{P}}$ shows that some prism phases (e.g., $\Phi_{4\mathcal{P}} = 0.668$, $\Phi_{4\triangle} = 0.627$, and $\Phi_{4\square} = 0.624$ at $z_{4\mathcal{P}}$) are more closely packed than the △ and □ phases at the same cell height but others (e.g., 3$\mathcal{P}$) are not. We point out that the smooth decay

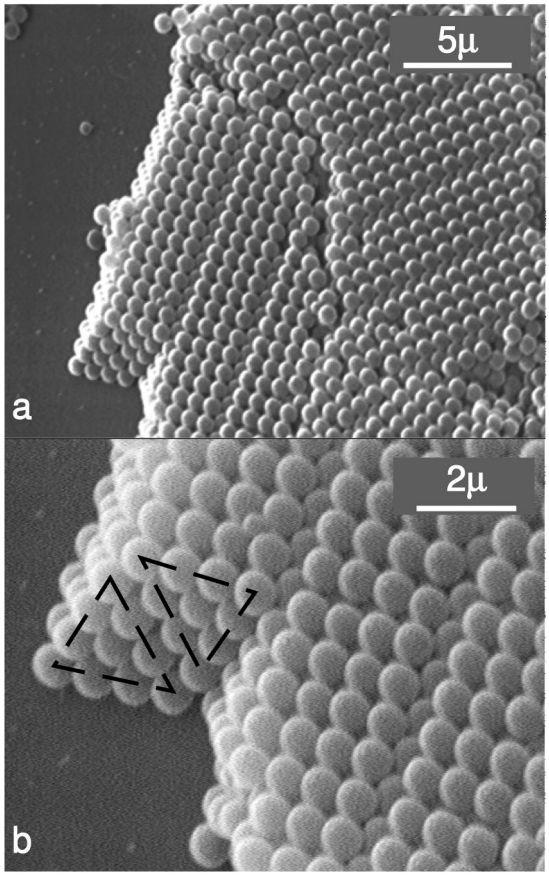

FIG. 3. (a) SEM image of two crystallites of the 4$\mathcal{P}$ phase separated by a phase boundary. The material missing in the left part of the image has been removed during preparation for the SEM. (b) Magnified view of the cross section visible in the lower left corner of (a). The contours of the prisms are added as a guide to the eye.

of the stripe pattern into the □ phase shown in Fig. 2 directly suggests a smooth transition between prism and □ phases. By use of a model of rigid prisms it can be visualized that a continuous transition among $n\square$, $n\mathcal{P}$, and $(n+1)\square$ is possible. This is sketched in Fig. 1(b) for the transition of $4\square \rightarrow 4\mathcal{P} \rightarrow 5\square$, where the prismlike buckling units are indicated by brighter and darker spheres, respectively. The sequence first shows the situation where the cell height *z* exactly matches the condition for the 4□ structure. With increasing *z* the brighter marked parts of the structures are dislocated somewhat in the vertical direction. This allows one to decrease the distance of adjacent prisms and therefore to increase Φ. Finally (bottom), when *z* is increased further this smooth transition leads to the 5□ structure.

To determine where these phases are expected to occur in the wedge, we calculated their packing fractions Φ and plotted them in Fig. 4 as a function of the cell height *z*. The symbols denote the situation when a particular structure exactly matches its optimum wedge height *z*. The dotted lines are taken from [12] and indicate how

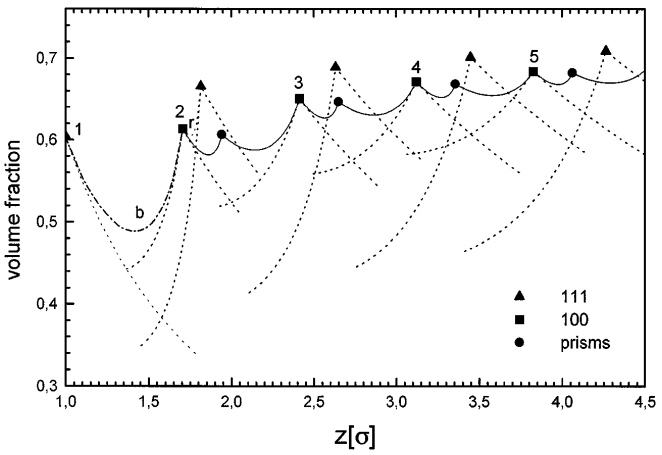

FIG. 4. Packing fraction vs height. The symbols indicate the height of a particular structure; the dotted lines show the decay of Φ when a structure does not match the wedge height (cf. [12]). The dash-dotted lines indicate the $1\triangle \rightarrow 2\square$ buckling transition and the rhombic phase taken from [16]. The full line is our calculation for the buckling transition between the $\square$ and the prism phases.

Φ for different structures decreases in the vicinity of their optimum z, and the dash-dotted lines are those for the buckling transition ($1\triangle \rightarrow 2\square$) and the rhombic phase ($2\square \rightarrow 2\triangle$) taken from [16]. Finally, the solid lines show the packing fractions of the prism phases, calculated according to our model. They show that the continuous transition is smoothing out the large fluctuations of Φ, which are present when only $\triangle$ and $\square$ phases are taken into account. Above this line there are peaks of the $\triangle$ phases, because none of the buckling structures exceeds their Φ when they match the wedge height exactly. The maximum increase of Φ is 4% ($4\square \rightarrow 4\triangle$) emphasizing the efficiency of the buckling process.

From Fig. 4 one obtains a prediction for the sequence of closest packed structures as a function of the cell height: $1\triangle$,$1\mathcal{B}$,$2\square$,$2r$,$2\triangle$,$2\mathcal{P}$,$3\square$,$3\mathcal{P}^{\star}$,$3\triangle$,$3\mathcal{P}$,$4\square$,$4\mathcal{P}$, $4\triangle$,$4\mathcal{P}$,.... This agrees well with the sequence found in the experiment pointing out that under our experimental conditions the packing fraction is maximized. The only exception is that the first appearance of the $3\mathcal{P}$ phase, marked with a star ($\star$), is not found in the experiment. Furthermore, a quantitative comparison with the experiment shows that the stability regime of the $\triangle$ and $\square$ phases is underestimated in Fig. 4. There are several reasons which may explain the deviations: First, the model is solely based on geometrical considerations and therefore cannot account for hysteresis effects and entropic contributions. However, according to Pansu *et al.* [12] the latter is qualified due to the fact that a hydrostatic pressure imposed on the particles largely reduces the influence of the entropic contributions to the free enthalpy and then the equilibrium configuration is that of maximum Φ. In our case the pressure is not hydrostatic but stems from the evaporation of the solvent during the experiment. Second, we added just one new class of structures to the model and of course there might be others. During our experiments we found hints on a buckling of structures with hexagonal basis which may account for the underestimated stability range of the $\triangle$ phases.

In conclusion we made experiments with nearly hard colloidal spheres subject to lateral compression within a wedge. We found a new buckling process, interpolating between $n\square$ and $(n+1)\square$ via a new intermediate prism phase $n\mathcal{P}$. The prism phases can be interpreted as fcc stacks with a periodic pattern of stacking faults. By means of this buckling process the system can adapt its structure to the local wall separation in order to maintain a high packing fraction.

We gratefully acknowledge helpful discussions with H. Löwen and M. Schmidt and financial support of the Deutsche Forschungsgemeinschaft (SFB 513).

[1] J. Kepler, *Strena, Seu, de Nive Sexangula* (G. Tampach, Frankfurt, 1611).
[2] J. H. Conway and N. J. A Sloane, *Sphere Packings, Lattices and Groups* (Springer, New York, 1993).
[3] For example, W. A. Gray, *The Packing of Solid Particles* (Chapman and Hall Ltd., London, 1968); S. V. Anishchik and N. N. Medvedev, Phys. Rev. Lett. **75**, 4314 (1995), and citations therein.
[4] C. F. Gauss, *Werke II* (Koniglichen Gesellschaft der Wissenschaften, Gottingen, 1876).
[5] W. Y. Hsiang, Int. J. Math. **4**, 739 (1993); Math. Intelligencer **17**, 35 (1995).
[6] A. H. Boerdeijk, Philips Res. Rep. **7**, 303 (1952).
[7] In our context "finite-size effects" are referred to as effects of small system size, i.e., when the system size becomes comparable to the particle diameter. This should not be mixed up with finite-size effects found in simulations, when the length scale of thermodynamic fluctuations approaches the size of the periodic boundary conditions.
[8] L. T. Wille and J. Vennik, J. Phys. A **18**, L419, L1113 (1985); R. Peikert, El. Math. **49**, 17 (1994).
[9] J. C. Crocker and D. G. Grier, J. Colloid Interface Sci. **179**, 298–310 (1996).
[10] P. Pieranski, L. Strzelecki, and B. Pansu, Phys. Rev. Lett **50**, 900 (1983).
[11] D. H. vanWinkle and C. A. Murray, Phys. Rev. A **34**, 562 (1986).
[12] B. Pansu, Pi. Pieranski, and Pa. Pieranski, J. Phys. (Paris) **45**, 331–339 (1984).
[13] S. Neser, T. Palberg, C. Bechinger, and P. Leiderer, Progr. Colloid Polym. Sci. **104**, 194 (1997).
[14] T. Ogawa, J. Phys. Soc. Jpn. Suppl. **52**, 167 (1983).
[15] Y. Koshikiya and S. Hachisu, in *Proceedings of the Colloid Symposium of Japan* (in Japanese, 1982).
[16] M. Schmidt and H. Löwen, Phys. Rev. Lett. **76**, 4552 (1996).
[17] T. Chou and D. R. Nelson, Phys. Rev. E **48**, 4611 (1993).